[Title] iTRVZ: liquid nano-platform for signal integration on the plasma membrane

Authors: Taka A. Tsunoyama[1], Christian Hoffmann[2], Bo Tang[1], Koichiro M. Hirosawa[3], Yuri L. Nemoto[1], Rinshi S. Kasai[3], Takahiro K. Fujiwara[4], Kenichi G.N. Suzuki[3,4], Dragomir Milovanovic[2], Akihiro Kusumi[1,4]*

Affiliations:

[1]Membrane Cooperativity Unit, Okinawa Institute of Science and Technology Graduate University (OIST); Onna-son, Okinawa, 904-0495, Japan.

[2]Laboratory of Molecular Neuroscience, German Centre for Neurodegenerative Diseases (DZNE); Berlin, 10117, Germany.

[3]Institute for Glyco-Core Research (iGCORE), Gifu University; Gifu, 501-1193, Japan.

[4]Institute for Integrated Cell-Material Sciences (WPI-iCeMS), Kyoto University; Kyoto, 606-8501, Japan.

*Corresponding author. Email: akihiro.kusumi@oist.jp

Abstract: Crosstalk of cellular signaling pathways is essential for coordinated cell responses. Therefore, we suspect the existence of scaffolding platforms that specifically undertake signal crosstalk and integration. Using advanced single-molecule imaging, we found a nanometer-scale liquid-like platform for integrating the signals downstream from GPI-anchored receptors and receptor-type tyrosine kinases. The platform employs some of the focal adhesion proteins, including integrin, talin, RIAM, VASP, and zyxin, but is distinct from focal adhesions, and is thus termed iTRVZ. The iTRVZ formation is driven by the protein liquid-liquid phase separation and the interactions with the raft domains in the plasma membrane and cortical actin. iTRVZ non-linearly integrates the two distinctly different receptor signals, and thus works as an AND gate and noise filter.

One-Sentence Summary: Nanometer-scale liquid-like protein platform for signal integration working as an AND gate was found on the plasma membrane.

Main Text:

Signaling pathways downstream from receptors are the targets of extensive investigations. In particular, understanding how each signaling pathway is integrated into coordinated cellular signal responses is one of the most critical issues in today's signaling research (*1*). We hypothesized that PM-associated structures that function as platforms for signal integration might exist. Since integrins are involved in the signaling of receptor-type tyrosine kinases (RTKs) (*2*), immunoglobulin E Fc receptor (*3*), and glycosylphosphatidylinositol (GPI)-anchored receptors (GPI-ARs), including CD59, Thy1, and CD55 (*4–9*), we examined the possibility that an integrin-centered signal integration platform might exist on the PM cytoplasmic surface.

Talin, a focal-adhesion (FA) protein, binds to integrins and various signaling molecules (*10*, *11*). We examined the possibility that talin might play a central role in the formation and function of the hypothetical signal integration platform. We expressed tagged-talin1 molecules (four different tags) in talin1/2 double-knockout mouse embryonic fibroblasts (dKO MEFs) (*11*), at levels comparable to that of endogenous talin1 (**fig. S1, A to K**). Our advanced single-molecule imaging revealed that fluorescently-labeled talin1 (talin; in the following, talin1 is described as talin) formed numerous clusters on the cytoplasmic surface of the *apical* PM, where virtually no FAs exist (*12*), even without stimulation (**fig. S1I, and movie S1**).

Clustered CD59, containing an average of five CD59 molecules mimicking the ligated signaling-active CD59 (*4*, *5*), and ligated PDGFR were transiently and repeatedly recruited to the talin clusters on the apical PM, with a dwell lifetime of each recruitment lasting for ~0.3 s (exponential decay time constant, τ_2; **Fig. 1, A and B, movies S2 and S3, and Materials and Methods**). The recruitments of these receptors suggested that the talin clusters might function as the signaling platform for both receptors.

We examined another FA protein, zyxin. Tagged zyxin proteins expressed at the level similar to that of endogenous zyxin in zyxin-KO MEF cells (*13*) also forms clusters on the *apical* PM (**fig. S1, E to I, and movie S1**). Each talin and zyxin cluster contains a median of 4.0 and 4.8 copies of talin and zyxin, respectively (with broad distributions between 2 and 15 copies/cluster) (**Fig. 1C**). These clusters exist on the apical PM densely, with a mean number density of ~0.25 clusters/μm^2 for both talin and zyxin (**Fig. 1D**). This number density is comparable to that of clathrin-coated structures (*14*).

Approximately 70% of the talin and zyxin clusters were colocalized with each other (**Fig. 1E, and fig. S1, J and K**, respectively), suggesting that these clusters are co-clusters of talin and zyxin. Meanwhile, this 70% colocalization of talin and zyxin clusters indicated that some of them might contain 0-2 copies of the talin and zyxin/cluster (the presence of 1~2 copies in the cluster could be missed under the employed imaging conditions). Zyxin and talin copy numbers

in each cluster vary greatly (**Fig. S1L**), indicating very high freedom of stoichiometry in the co-clusters. Allowing high flexibilities in stoichiometry for incorporating various molecules would be an important feature as the signaling platform.

We refer to these altogether as "talin-zyxin clusters". Partial actin depolymerization with latrunculin A and cytochalasin D, and myosin deactivation with the ROCK inhibitor Y27632 reduced both the number density of talin clusters in the apical PM and the number of talin molecules within a talin cluster, suggesting that the formation of the talin-zyxin clusters requires the intact actin-myosin system. Meanwhile, stimulation by CD59 clustering or PDGF addition did not induce any changes in either the talin cluster number density or the talin number within a cluster (**Fig. 1, C and D**).

The lifetime of the talin-zyxin clusters exhibited the presence of two components (**Fig. 1F**): ~15% lasted for ~1 s and ~85% lasted for ~10 s (arithmetic means of talin and zyxin lifetimes). These lifetimes would represent both the decomposition of the clusters and the dissociation of the clusters from the apical PM. Meanwhile, the lifetime of talin clusters without zyxin observed in the zyxin-KO MEFs and the lifetime of zyxin clusters without talin in talin-dKO MEFs were both 1.1 s, and after rescue, the lifetimes became 9.5 s and 7.7 s, respectively (**Fig. S1M**; all SEM values given in figures). These results indicate that the ~1-s component (~15%) of the talin-zyxin clusters represents those that do not contain either talin or zyxin. The value of 85% for the 7.7~9.5-s component is indeed close to the 70% estimated for the clusters containing both (more than two) talin and zyxin proteins.

Single molecules of talin and zyxin repeatedly entered and exited from the clusters, with dwell lifetimes in the talin-zyxin cluster of 2.1 and 1.4 s, respectively (**Fig. 1G, and fig. S1N**), indicating that these molecules exchange with those in the bulk cytoplasm several times during the lifetime of the talin-zyxin cluster. This result indicates the liquid-like characteristics of the clusters.

Photoactivation localization microscopy (PALM) of talin and zyxin in fixed cells, followed by a Voronoï tessellation analysis (*15, 16*), detected their nanoscale clusters (median diameter = 60 nm) on the *apical* PM at a number density of 0.35 clusters/μm^2 (mean; the average for talin and zyxin) (**Fig. 1, H to K, and fig. S2, A to G**), consisting of a mean of 6.1 and 8.2 copies of talin and zyxin, respectively (slightly overestimated because clusters containing fewer than 3 copies were undetectable; **Fig. 1J**).

In summary, talin-zyxin clusters are liquid-like, nanoscale clusters with a lifetime on the PM of ~10 s, where constituent molecules and engaged receptors (PDGFR and CD59) are exchanging on the time scale of 0.3 - 2.1 s (see the intensity fluctuations of the cluster in **movie S4**). Talin-zyxin clusters were found in all five cell lines examined here (**fig. S3A**), suggesting that these clusters broadly exist in mammalian cells.

To facilitate the observations of single-molecule recruitment to the talin-zyxin clusters in the *apical PM*, we employed a human T24 epithelial cell line, because the apical PM of the T24 cell is quite flat, facilitating single-molecule imaging (**fig. S3, B to E**). We generated the T24 cells stably expressing SNAPf-talin (called T24-T; together with endogenous talin1, expressing 1.7x more talin than that in wild-type cells). As in MEFs, the engaged CD59 and PDGFR were transiently recruited to the talin-zyxin clusters in T24-T cells (**fig. S3, F to I**).

We next investigated the presence of other FA proteins in the talin-zyxin clusters (**fig. S3J**). To systematically evaluate the propensity of the FA proteins to colocalize with the talin-zyxin clusters at the level of single molecules, we employed the "colocalization index", which is a measure of finding a molecule within a 50 nm radius circle around the center of the talin cluster relative to far distances *(17)* (as a control, all fluorescent spots were shifted by 1 μm with random angles in 2D) (**fig. S3K, and Materials and Methods**). β3 integrin (i), RIAM (R), VASP (V), and zyxin (Z) were remarkably colocalized with the talin (T) clusters even before PDGF stimulation, and therefore, we coined the name iTRVZ for the talin-zyxin cluster. Meanwhile, paxillin, vinculin, and N-WASP were not colocalized, showing that although iTRVZ contains FA proteins, its protein composition is distinct from that of the mature FA *(18)* (**Fig. 2A**). The actin-binding proteins α-actinin and filamin were also colocalized with iTRVZ. Upon PDGF stimulation, interestingly, the colocalizations of the T, R, V, and Z proteins were not increased, whereas those of integrin and FAK were increased (**Fig. 2A**). Consistently, the dwell lifetime of FAK at the iTRVZ was elongated (**fig. S3, L and M, and movie S5**). Furthermore, paxillin and N-WASP were recruited to iTRVZ after stimulation.

The PDGF stimulation induced the iTRVZ recruitment of FAK, PLCγ1, Lyn, PI3K, and Akt (**Fig. 2, A and B**). Furthermore, PLCγ1 was transiently recruited to iTRVZ upon the engagements of GPI-ARs (CD59 and Thy1) and RTKs (PDGFR and EGFR), and PLCβ was recruited upon the stimulation of a GPCR (UTP receptor, P2Y) (**Fig. 2, C and D**). The recruitment of these molecules was reduced by the inhibitors for FAK and SFK (**Fig. 2C**, however, EGF stimulation after FAK inhibitor treatment and UTP stimulation after both inhibitor treatments showed moderate reduction without significant differences). The PDGF-induced PLCγ1 recruitment additionally occurred on the PM outside the iTRVZ (**fig. S3, N and O**), indicating that the PDGFR's downstream signal occurs both inside and outside the iTRVZ. However, the PLCγ1's recruitment per unit area is ~30 times greater in the iTRVZ than in the region outside the PM (**Fig. 2E**, see also **fig. S3, N and O**), indicating that the signaling reactions would occur much more efficiently in iTRVZ (**Fig. 2F**). As such, iTRVZ works as a platform for various signaling pathways.

The involvement of phosphoinositides in iTRVZ was examined because PLCγ1 is recruited to iTRVZ, and talin and RIAM bind PI(4,5)P_2 *(19, 20)* (**Fig. 3, A to C, and movie S6**). Using

probes for various phosphoinositides (*21*), PI(4)P and PI(4,5)P_2, but not PI(3)P and PI(3,4)P_2, were localized at the iTRVZ both before and after PDGF stimulation equally, but PI(3,4,5)P_3 was found only after stimulation (**Fig. 3C**). PI3K, which generates PI(3,4,5)P_3 from PI(4,5)P_2, was recruited to the iTRVZ only after PDGF stimulation (**Fig. 2B**), whereas PIP5K, which generates PI(4,5)P_2 and binds to talin (*19*) and MARCKS, a PI(4,5)P_2-sequestering protein, were recruited even before stimulation without any changes after stimulation. These results suggest that PI(3,4,5)P_3 is generated from PI(4,5)P_2 by the PI3K recruited to iTRVZ upon stimulation.

Meanwhile, typical raftophilic lipids, cholesterol and sphingomyelin (SM), were colocalized with the iTRVZ (*22*, *23*) (**Fig. 3, B and C**). The number density and size (talin number) of the iTRVZ were reduced after partial depletions of cholesterol and PI(4,5)P_2 (*4*, *5*, *24*, *25*) (**fig. S4, A to K**). Phosphatidylserine (PS), with its long, saturated acyl chain subfraction putatively involved in the aster formation of GPI-ARs and actin filaments (*9*, *26*, *27*), was also colocalized with the iTRVZ (**Fig. 3C**). These results suggest that iTRVZ is supported by raft-lipid interactions (*28*) by way of PI(4,5)P_2 (and possibly long, saturated-chain PS). Meanwhile, the RTK's downstream signaling molecules JAK1, K-Ras, and Raf were not recruited to the iTRVZ (**Fig. 3D**).

In conclusion, iTRVZ, formed with the aid of raft domains by way of PI(4,5)P_2 and PS, recruits various signaling molecules downstream from the activated receptors, and works as the signal transduction platform for GPI-ARs, RTKs, and GPCRs (**Fig. 3E**). Namely, iTRVZ is shared by these receptor signaling pathways, suggesting the possibility that signal crosstalk and integration are induced there.

Indeed, iTRVZ cooperatively and non-linearly integrates the PDGFR (RTK) and CD59 (GPI-AR) signals. First, we weakly stimulated the cells by adding either 20 pM PDGF (physiological concentration in the serum (*29*)) or 20 nM anti-CD59 mAb coated beads for CD59 clustering, which are 1/1,000 and 1/100 concentrations of our standard conditions, respectively. They induced much lower PLCγ1 recruitment to the iTRVZ and Ca^{2+} responses than those in our standard conditions (**Fig. 4, A and B, and fig. S5A**). When we added both stimulants at the same time, the PLCγ1 recruitment to iTRVZ and the Ca^{2+} responses became greater than the sum of those induced by separate stimulations, by factors of 4.7 and 6.8, respectively (**Fig. 4, A and B, and fig. S5A**), clearly demonstrating the cooperative, non-linear integration of the two signals.

This non-linear integrated amplification depended on iTRVZ, because it did not happen with zyxin-KO cells. However, it was recovered by the addition of the intrinsically disordered region [IDR] of zyxin, which is responsible for the formation of zyxin-talin co-clusters (**Fig. 4, A and B, and fig. S5, B and C;** for the zyxin's IDR, see the next subsection).

The non-linear integration depended on the activation of both FAK and SFK at iTRVZ (**Fig. 4, A and B, and fig. 5C**), and did not occur outside the iTRVZ (**Fig. 4B**). Since the weak CD59 stimulation induced the FAK recruitment to iTRVZ more effectively than the SFK

recruitment, and the weak PDGF stimulation triggered SFK recruitment but not the FAK recruitment (**fig. 5D**), the cooperative integration is considered to be induced by the simultaneous recruitment of SFK and FAK to iTRVZ, causing their upward spiral activations (**Fig. 4C, and fig. S5E**). In conclusion, iTRVZ works as a cooperative signal integrator for multiple, coincidental signals due to the co-activation of SFK and FAK in the fluid nano-region.

The iTRVZ's main constituent molecules, RIAM, VASP, and zyxin, contain long intrinsically disordered regions (IDRs) (*30*) (**Fig. 4D, and fig. S6, A and B**), which are often involved in liquid-liquid phase separation (LLPS) (*31–34*). Therefore, we examined the involvement of LLPS in iTRVZ formation.

First, iTRVZ was reduced in size (the talin number) in MEF cells after a 1,6-hexanediol treatment, which is known to disperse liquid condensates (**Fig. 1C**). Second, purified zyxin and VASP formed micron-scale liquid-like co-condensates *in vitro* at endogenous concentrations of 0.7~3.0 and 0.25 ~0.7 μM, respectively (**Fig. 4, E and F, and fig. S7, A to J**), indicating that zyxin and VASP are capable of undergoing LLPS. In T24 cells, micron-scale condensates of zyxin and VASP were never observed at endogenous expression levels, but were formed (always co-clustered) in cells overexpressing the proteins at ~14 μM average concentrations in the cytoplasm (**Fig. 4, G and H, fig. S7, K to M, and movie S7**), probably due to the presence of higher concentrations of proteins and other electrolytes like ATP (*35*). The results obtained using WT and mutant zyxin (**Fig. 4D**), as well as those of VASP and RIAM, showed that the non-phosphorylated IDR domains are essential for their recruitment to iTRVZ (**Fig. 4I, and fig. S8, A and B**).

To further examine the IDR involvement in iTRVZ formation and signal transduction, we produced seven zyxin-KO MEF cell lines expressing different zyxin mutants (**fig. S9, A to F**). By comparing the sizes (talin numbers) and lifetimes of the iTRVZ in these cell lines (**fig. S9, D and E**), we found that the dephosphorylated IDR (including the Pro-rich domain) of zyxin enhance iTRVZ formation. Upon PDGF stimulation, the four cell lines expressing zyxin lacking IDRs or expressing phosphomimetic zyxin exhibited lower Ca^{2+} responses and Akt phosphorylation, as compared with the zyxin-KO MEF cells rescued with the full-length zyxin (**Fig. 4, J to L, and fig. S9, G and H**). As described in the previous subsection, the non-linear integration of the weak CD59 and PDGF signals did not occur in cells without zyxin expression, but was recovered by expressing zyxin's IDR (**Fig. 4B, and fig. S5A**). In conclusion, these data demonstrate that the IDR-based LLPS is critical for generating the functional iTRVZ platform.

We identified a nanoscale liquid-like signal integration platform on the PM, iTRVZ (**fig. S10**), which exists in both the apical and basal PMs. The iTRVZ platform is commonly used for the signaling pathways of three representative receptor classes: GPI-AR (CD59, Thy1), RTK (PDGFR, EGFR), and GPCR (UTP receptor, P2Y) (**Fig. 2C**). The recruited receptors and

downstream signaling molecules would interact at iTRVZ extremely rapidly and efficiently, due to the very small sizes of the iTRVZ platform (50 ~ 80 nm in diameter) and its liquid nature.

iTRVZ works as a cooperative and non-linear integrator and coincidence detector/amplifier of the signals from these different signaling pathways. Non-linear integration and coincidence detection/amplification would be critically important for inducing strong downstream signals when two separate external signals are received by the cell at about the same time, as well as for filtering out the accidentally evoked noise that would be prevalent in the cytoplasm (*36*, *37*).

The lifetime of iTRVZ is ~10 s, and its constituent molecules and recruited receptors and signaling molecules exchange with those in the bulk cytoplasm in the time scale of 0.2 - 3 s (**Fig. 1F and fig. S1L**), although the overall receptor signal in a whole cell tends to last for several minutes or longer. This indicates that each iTRVZ platform would create unit pulse-like signals on the order of seconds, and that the signal observed for a whole single cell, like the phosphorylation levels and Ca^{2+} mobilization, would be the result of the summation of the unit pulse-like signals from many iTRVZ (*4*, *5*, *38*, *39*). In addition, the limited iTRVZ lifetime and dwell lifetimes of signaling molecules would be useful for turning off the signals quickly and reliably: the output signal from each iTRVZ would be stopped within ~10 s without fail because iTRVZ will self-destruct and/or self-dissociate from the PM in 10 s. Similar transient liquid-like nanoscale signaling platforms might exist for other signaling systems (*34*, *40*) including those in immune cells (*3*, *40*).

The iTRVZ is probably formed by LLPS due to the IDR-IDR interactions of zyxin and VASP, and perhaps those of RIAM and other constituent molecules (**Fig. 4, D to I, and figs. S7 to 9**). The protein LLPS condensates on the nanometer scale have been suggested recently (*41*). The iTRVZ is interfaced with the raft domains by way of $PI(4,5)P_2$, and possibly PS with long, saturated acyl chains (*26*). The enhanced 3D protein LLPS on the raft domain surface has been suggested recently (*42*).

For the iTRVZ functions, the liquid-like properties of iTRVZ with loose stoichiometries, supported by the IDR-based LLPS, would be critically important. They would make iTRVZ quite versatile, to allow for the recruitment of a variety of receptors (some RTKs might participate in LLPS (*43*)) and signaling molecules without strict stoichiometric limitations, the enhancement of their interactions, their rapid departures from iTRVZ, and its self-destruction in 10 s. In the basal PM, some of the iTRVZs might convert into nano-scale nascent FAs upon the applied stress via integrin and vinculin recruitment (*9*, *10*, *18*, *44*). iTRVZ was found in all of the cell lines examined in this study, and thus we conclude that it is a fundamentally important signal integration platform ubiquitously functioning in mammalian cells.

References and Notes

1. C. M. Taniguchi, B. Emanuelli, C. R. Kahn, Critical nodes in signalling pathways: insights into insulin action. *Nat. Rev. Mol. Cell Biol.* 7, 85–96 (2006).

2. Z. Chen, D. Oh, A. K. Dubey, M. Yao, B. Yang, J. T. Groves, M. Sheetz, EGFR family and Src family kinase interactions: mechanics matters? *Curr. Opin. Cell Biol.* 51, 97–102 (2018).

3. D. L. Wakefield, D. Holowka, B. Baird, The FcεRI signaling cascade and integrin trafficking converge at patterned ligand surfaces. *Mol. Biol. Cell*. 28, 3383–3396 (2017).

4. K. G. N. Suzuki, T. K. Fujiwara, M. Edidin, A. Kusumi, Dynamic recruitment of phospholipase Cγ at transiently immobilized GPI-anchored receptor clusters induces IP_3–Ca^{2+} signaling: single-molecule tracking study 2. *J. Cell Biol.* 177, 731–742 (2007).

5. K. G. N. Suzuki, T. K. Fujiwara, F. Sanematsu, R. Iino, M. Edidin, A. Kusumi, GPI-anchored receptor clusters transiently recruit Lyn and Gα for temporary cluster immobilization and Lyn activation: single-molecule tracking study 1. *J. Cell Biol.* 177, 717–730 (2007).

6. X. Cui, X. Zhang, H. Bu, N. Liu, H. Li, X. Guan, H. Yan, Y. Wang, H. Zhang, Y. Ding, M. Cheng, Shear stress-mediated changes in the expression of complement regulatory protein CD59 on human endothelial progenitor cells by ECM-integrinαVβ3-F-actin pathway in vitro. *Biochem. Biophys. Res. Commun.* 494, 416–421 (2017).

7. R. J. Morris, Thy-1, a pathfinder protein for the post-genomic era. *Front. Cell Dev. Biol.* 6, 173 (2018).

8. M. G. Strainic, J. Liu, F. An, E. Bailey, A. Esposito, J. Hamann, P. S. Heeger, M. E. Medof, CD55 is essential for $CD103^+$ dendritic cell tolerogenic responses that protect against autoimmunity. *Am. J. Pathol.* 189, 1386–1401 (2019).

9. J. M. Kalappurakkal, A. A. Anilkumar, C. Patra, T. S. van Zanten, M. P. Sheetz, S. Mayor, Integrin mechano-chemical signaling generates plasma membrane nanodomains that promote cell spreading. *Cell*. 177, 1738-1756. e23 (2019).

10. P. Kanchanawong, G. Shtengel, A. M. Pasapera, E. B. Ramko, M. W. Davidson, H. F. Hess, C. M. Waterman, Nanoscale architecture of integrin-based cell adhesions. *Nature*. 468, 580–584 (2010).

11. M. Theodosiou, M. Widmaier, R. T. Böttcher, E. Rognoni, M. Veelders, M. Bharadwaj, A. Lambacher, K. Austen, D. J. Müller, R. Zent, R. Fässler, Kindlin-2 cooperates with talin to activate integrins and induces cell spreading by directly binding paxillin. *eLife*. 5, e10130 (2016).

12. K. M. Yamada, M. Sixt, Mechanisms of 3D cell migration. *Nat. Rev. Mol. Cell Biol.* 20, 738–752 (2019).

13. L. M. Hoffman, C. C. Jensen, S. Kloeker, CL. A. Wang, M. Yoshigi, M. C. Beckerle, Genetic ablation of zyxin causes Mena/VASP mislocalization, increased motility, and deficits in actin remodeling. *J. Cell Biol.* 172, 771–782 (2006).

14. T. K. Fujiwara, K. Iwasawa, Z. Kalay, T. A. Tsunoyama, Y. Watanabe, Y. M. Umemura, H. Murakoshi, K. G. N. Suzuki, Y. L. Nemoto, N. Morone, A. Kusumi, Confined diffusion of transmembrane proteins and lipids induced by the same actin meshwork lining the plasma membrane. *Mol. Biol. Cell*. 27, 1101–1119 (2016).

15. P. Sengupta, S. Van Engelenburg, J. Lippincott-Schwartz, Visualizing cell structure and function with point-localization superresolution imaging. *Dev. Cell*. 23, 1092–1102 (2012).

16. F. Levet, E. Hosy, A. Kechkar, C. Butler, A. Beghin, D. Choquet, J.-B. Sibarita, SR-Tesseler: a method to segment and quantify localization-based super-resolution microscopy data. *Nat. Methods*. 12, 1065–1071 (2015).

17. M. B. Stone, S. L. Veatch, Steady-state cross-correlations for live two-colour super-resolution localization data sets. *Nat. Commun.* 6, 7347 (2014).

18. S. J. Han, E. V. Azarova, A. J. Whitewood, A. Bachir, E. Guttierrez, A. Groisman, A. R. Horwitz, B. T. Goult, K. M. Dean, G. Danuser, Pre-complexation of talin and vinculin without tension is required for efficient nascent adhesion maturation. *eLife*. 10, e66151 (2021).

19. G. D. Paolo, L. Pellegrini, K. Letinic, G. Cestra, R. Zoncu, S. Voronov, S. Chang, J. Guo, M. R. Wenk, P. D. Camilli, Recruitment and regulation of phosphatidylinositol phosphate kinase type 1γ by the FERM domain of talin. *Nature*. 420, 85–89 (2002).

20. EA. Cho, P. Zhang, V. Kumar, M. Kavalchuk, H. Zhang, Q. Huang, J. S. Duncan, J. Wu, Phosphorylation of RIAM by src promotes integrin activation by unmasking the PH domain of RIAM. *Structure*. 29, 320-329. e4 (2021).

21. M. Furutani, K. Tsujita, T. Itoh, T. Ijuin, T. Takenawa, Application of phosphoinositide-binding domains for the detection and quantification of specific phosphoinositides. *Anal. Biochem.* 355, 8–18 (2006).

22. M. Maekawa, Domain 4 (D4) of perfringolysin O to visualize cholesterol in cellular membranes—the update. *Sensors*. 17, 504 (2017).

23. S. Endapally, D. Frias, M. Grzemska, A. Gay, D. R. Tomchick, A. Radhakrishnan, Molecular discrimination between two conformations of sphingomyelin in plasma membranes. *Cell*. 176, 1040-1053. e17 (2019).

24. O. Idevall-Hagren, E. J. Dickson, B. Hille, D. K. Toomre, P. D. Camilli, Optogenetic control of phosphoinositide metabolism. *Proc. Natl. Acad. Sci. USA*. 109, E2316–E2323 (2012).

25. M. de S. Santos, R. M. Z. G. Naal, B. Baird, D. Holowka, Inhibitors of PI(4,5)P_2 synthesis reveal dynamic regulation of IgE receptor signaling by phosphoinositides in RBL mast cells. *Mol. Pharmacol.* 83, 793–804 (2013).

26. K. Gowrishankar, S. Ghosh, S. Saha, C. Rumamol, S. Mayor, M. Rao, Active remodeling of cortical actin regulates spatiotemporal organization of cell surface molecules. *Cell*. 149, 1353–1367 (2012).

27. S. Lee, Y. Uchida, J. Wang, T. Matsudaira, T. Nakagawa, T. Kishimoto, K. Mukai, T. Inaba, T. Kobayashi, R. S. Molday, T. Taguchi, H. Arai, Transport through recycling endosomes requires EHD1 recruitment by a phosphatidylserine translocase. *EMBO J.* 34, 669–688 (2015).

28. K. Simons, J. L. Sampaio, Membrane organization and lipid rafts. *Cold Spring Harb. Perspect. Biol.* 3, a004697 (2011).

29. E. Rossi, B. Casali, G. Regolisti, S. Davoli, F. Perazzoli, A. Negro, C. Sani, B. Tumiati, D. Nicoli, Increased plasma levels of platelet-derived growth factor (PDGF-BB + PDGF-AB) in patients with never-treated mild essential hypertension. *Am. J. Hypertens.* 11, 1239–1243 (1998).

30. D. Piovesan, M. Necci, N. Escobedo, A. M. Monzon, A. Hatos, I. Mičetić, F. Quaglia, L. Paladin, P. Ramasamy, Z. Dosztányi, W. F. Vranken, N. E. Davey, G. Parisi, M. Fuxreiter, S. C. E. Tosatto, MobiDB: intrinsically disordered proteins in 2021. *Nucleic Acids Res.* 49, D361–D367 (2020).

31. D. Milovanovic, Y. Wu, X. Bian, P. D. Camilli, A liquid phase of synapsin and lipid vesicles. *Science*. 361, eaat5671 (2018).

32. Z. Feng, X. Chen, X. Wu, M. Zhang, Formation of biological condensates via phase separation: Characteristics, analytical methods, and physiological implications. *J. Biol. Chem.* 294, 14823–14835 (2019).

33. L. B. Case, J. A. Ditlev, M. K. Rosen, Regulation of transmembrane signaling by phase separation. *Annu. Rev. Biophys.* 48, 1–30 (2019).

34. K. Jaqaman, J. A. Ditlev, Biomolecular condensates in membrane receptor signaling. *Curr. Opin. Cell Biol.* 69, 48–54 (2021).

35. C. Hoffmann, R. Sansevrino, G. Morabito, C. Logan, R. M. Vabulas, A. Ulusoy, M. Ganzella, D. Milovanovic, Synapsin condensates recruit alpha-synuclein. *J. Mol. Biol.* 433, 166961 (2021).

36. W. Y. C. Huang, S. Alvarez, Y. Kondo, Y. K. Lee, J. K. Chung, H. Y. M. Lam, K. H. Biswas, J. Kuriyan, J. T. Groves, A molecular assembly phase transition and kinetic proofreading modulate Ras activation by SOS. *Science*. 363, 1098–1103 (2019).

37. A. Klosin, F. Oltsch, T. Harmon, A. Honigmann, F. Jülicher, A. A. Hyman, C. Zechner, Phase separation provides a mechanism to reduce noise in cells. *Science*. 367, 464–468 (2020).

38. K. G. N. Suzuki, R. S. Kasai, K. M. Hirosawa, Y. L. Nemoto, M. Ishibashi, Y. Miwa, T. K. Fujiwara, A. Kusumi, Transient GPI-anchored protein homodimers are units for raft organization and function. *Nat. Chem. Biol.* 8, 774–783 (2012).

39. A. Kusumi, T. A. Tsunoyama, K. M. Hirosawa, R. S. Kasai, T. K. Fujiwara, Tracking single molecules at work in living cells. *Nat. Chem. Biol.* 10, 524–532 (2014).

40. X. Su, J. A. Ditlev, E. Hui, W. Xing, S. Banjade, J. Okrut, D. S. King, J. Taunton, M. K. Rosen, R. D. Vale, Phase separation of signaling molecules promotes T cell receptor signal transduction. *Science*. 352, 595–599 (2016).

41. S. Peng, W. Li, Y. Yao, W. Xing, P. Li, C. Chen, Phase separation at the nanoscale quantified by dcFCCS. *Proc. Natl Acad. Sci. USA*. 117, 27124–27131 (2020).

42. M. Rouches, S. L. Veatch, B. B. Machta, Surface densities prewet a near-critical membrane. *Proc. Natl. Acad. Sci. USA*. 118, e2103401118 (2021).

43. CC. Lin, K. M. Suen, PA. Jeffrey, L. Wieteska, J. A. Lidster, P. Bao, A. P. Curd, A. Stainthorp, C. Seiler, H. Koss, E. Miska, Z. Ahmed, S. D. Evans, C. Molina-París, J. E. Ladbury, Receptor tyrosine kinases regulate signal transduction through a liquid-liquid phase separated state. *Mol. Cell*. 82, 1089-1106. e12 (2022).

44. S. Massou, F. N. Vicente, F. Wetzel, A. Mehidi, D. Strehle, C. Leduc, R. Voituriez, O. Rossier, P. Nassoy, G. Giannone, Cell stretching is amplified by active actin remodelling to deform and recruit proteins in mechanosensitive structures. *Nat. Cell Biol.* 22, 1011–1023 (2020).

Acknowledgments: We thank the PIs for the kind gifts of cell lines and cDNAs (details are given in the supplementary text). We also thank Drs. P. Kanchanawong, S. Liu, and M. Kham (National University of Singapore) for the technical support for the mouse embryonic stem cell culture, Drs. P. Barzaghi and B. Humbel (OIST Imaging Section) for supporting FRAP experiments, and Drs. K. Simons (Lipotype GmbH), S. Mayor (National Centre for Biological Sciences), and all members of the Kusumi laboratory for valuable discussions.

Funding:

Japan Society for the Promotion of Science (JSPS) Grants-in-Aid for Scientific Research Kiban A 21H04772 (AK)

JSPS Grants-in-Aid for Scientific Research Kiban S 16H06386 (AK)

JSPS Grants-in-Aid for Scientific Research Kiban A 21H04772 (AK)

JSPS Grants-in-Aid for Scientific Research Kiban B 16H04775 (TKF)

JSPS Grants-in-Aid for Scientific Research Kiban C 17K07333 (RSK)

JSPS Grants-in-Aid for Scientific Research Wakate B 26870292 (RSK)

JSPS Grants-in-Aid for Scientific Research Wakate 21K15058 (TAT)

JSPS Challenging Exploratory Research 18K19001 (TKF)

Grant-in-Aid for Innovative Areas from the Ministry of Education, Culture, Sports, Science and Technology of the Japanese government (MEXT) 18H04671 (KGNS)

Japan Science and Technology Agency (JST) grant in the program of the Core Research for Evolutional Science and Technology (CREST) in the field of "Biodynamics" (AK)

JST grant in the program of CREST in the field of "Extracellular Fine Particles" JPMJCR18H2 (KGNS)

JST grant ACT-X JPMJAX211B (TAT)

WPI-iCeMS of Kyoto University is supported by the World Premiere Research Center Initiative (WPI) of MEXT.

Author contributions: T.A.T. performed large majorities of the single-fluorescent-molecule imaging, biochemical, and molecular biology experiments and analyses. T.A.T., T.K.F., and A.K. developed the single-molecule imaging camera system, set up single-molecule imaging stations, and developed the analysis software. C.H. and D.M purified zyxin and VASP and, together with T.A.T., performed LLPS and FRAP experiments. B.T. generated protein probes for cholesterol and sphingomyelin. T.A.T., Y.L.N., K.M.H., R.S.K., T.K.F., K.G.N.S., C.H., D.M., and A.K. participated in discussions throughout the course of this research. T.A.T., T.K.F., K.G.N.S., and A.K. conceived and formulated this project, and evaluated and discussed data. T.A.T. and A.K. wrote the manuscript and all authors participated in its revision.

Competing interests: The authors declare no competing financial interests.

Data and materials availability: All data are available in the main text or the supplementary materials.

Supplementary Materials

Materials and Methods

Figs. S1 to S10

References (*43–141*)

Movies S1 to S7

Data S1 to S2

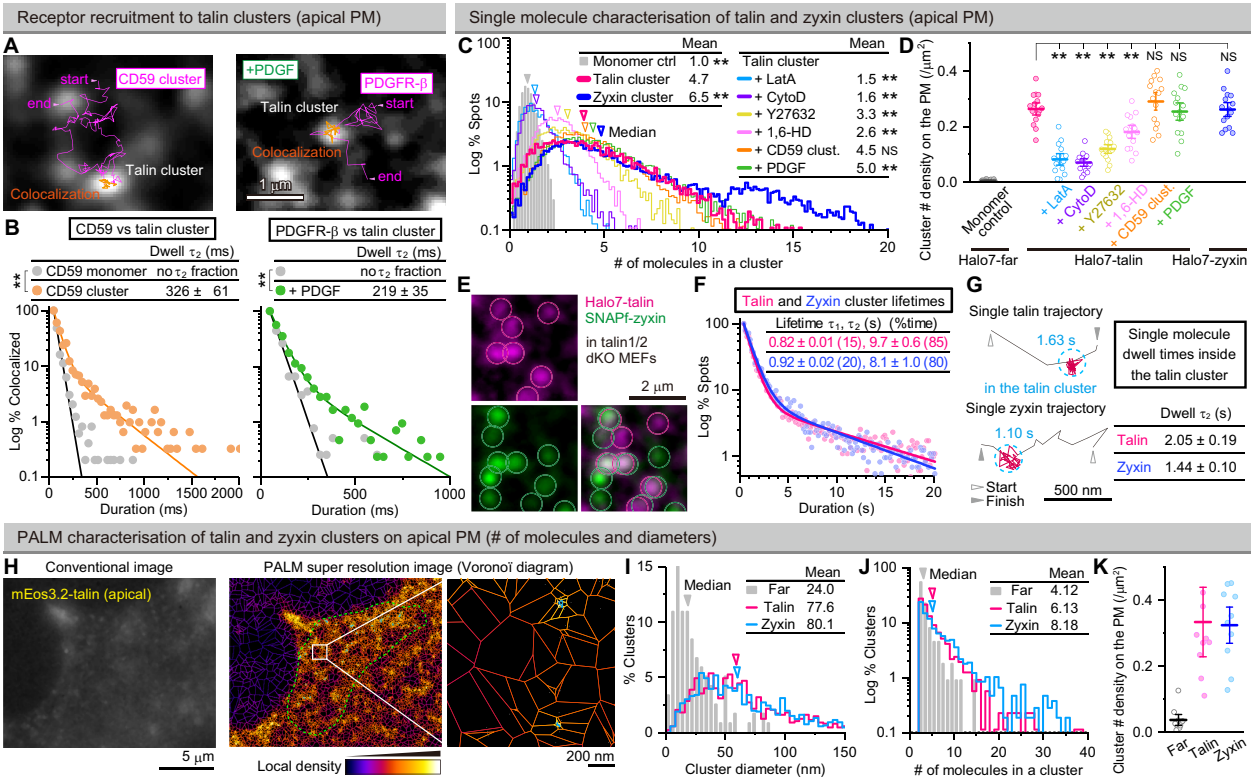

Fig. 1. Co-clusters of talin and zyxin with ~10-s lifetimes on the apical PM recruit receptors.

(**A** and **B**) Engaged CD59 (clustered by a fluorescent bead coated with anti-CD59 mAb) and Halo7-PDGFR (trajectories) were recruited to SNAPf-talin clusters (white spots in (A)) with dwell lifetimes of 0.33 and 0.22 s, respectively (B) (**movies S2 and S3**). Throughout this work, we found that the dwell time distributions could be fitted by double exponential functions, and the longer decay time constants, τ_2, provided biologically meaningful lifetimes (**the main text, and Materials and Methods**), while the fitting error provided the SEM (n_{cells} = 20, n_{events} = 955, 1,046, 758, and 1,094 for CD59 mononer, CD59 cluster, –PDGF, and +PDGF, respectively).

(**C**) Distributions of the numbers of Halo7-tagged molecules residing in each cluster (monomer control: farnesylated Halo7 [Halo7-far], n_{cells} = 15, n_{spots} = 2,415 ~ 10,780).

(**D**) Number densities of Halo7-tagged talin and zyxin clusters on the apical PM (dots for individual cells; bars for mean ± SEM, n_{cells} = 15).

(**E**) Typical dual color images of talin and zyxin clusters (indicated by circles); ~70% clusters are colocalized with each other (**fig. S1, J and K**).

(**F**) Lifetime distributions of individual Halo7-tagged clusters (n_{cells} = 10, n_{spots} = 7,407 and 6,888 for talin and zyxin, respectively).

(**G**) Typical trajectories of single Halo7-talin and SNAPf-zyxin molecules, exhibiting their temporary recruitment (magenta trajectories) to talin clusters (cyan circles). Their dwell lifetimes are also shown (**fig. S1N**).

(**H**) Conventional and PALM super-resolution images (Voronoï diagram) of mEos3.2-talin on the apical PM. The areas surrounded by the green curve (image in the middle) were the regions with good focus (the apical PM is tilted variously) and used for further analysis. The cyan lines in the image on the right indicate the smallest polygon that included the clustered spots.

(**I** to **K**) Distributions of the cluster diameters (I), the copy numbers of molecules in a cluster (J; cf. C)), and number densities of the clusters on the apical PM (K) (**n_{cells}** = 10, $n_{clusters}$ = 113, 877, and 1,065 for far, talin, and zyxin, respectively).

NS, not significant, *, $P < 0.05$, **, $P < 0.01$, using Brunner-Munzel test for (B), Steel-Dwass' test for (C, vs Talin cluster), and Games-Howell's test for (D).

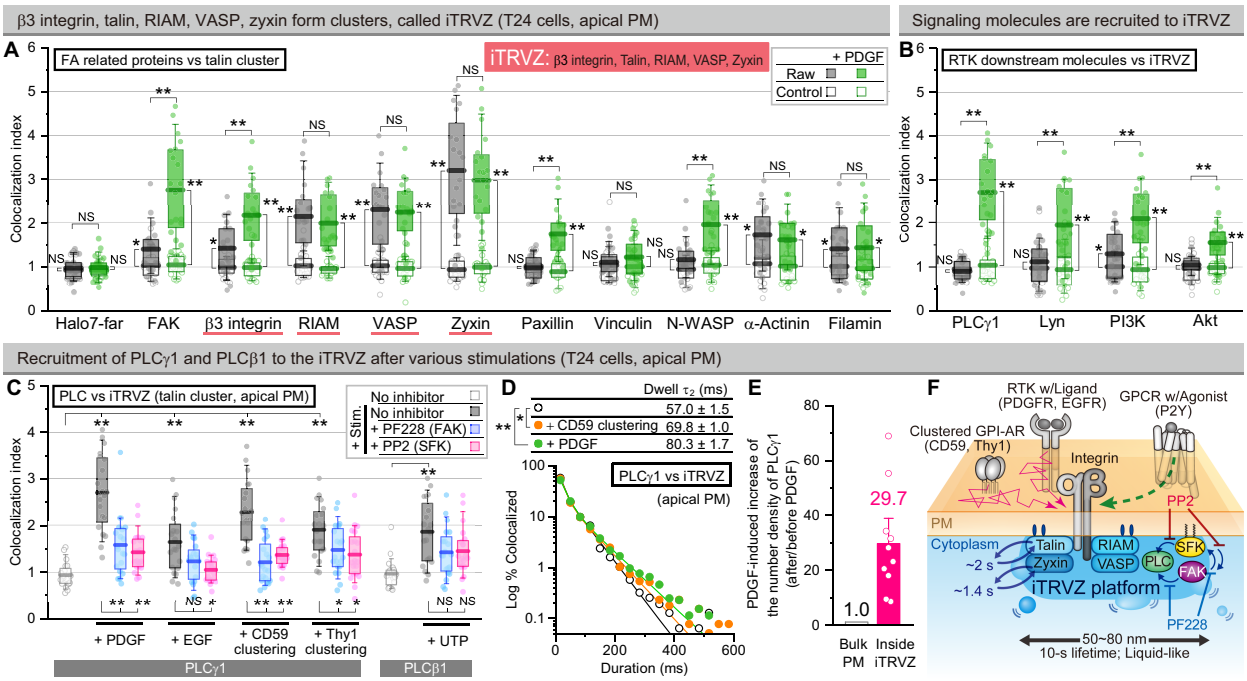

Fig. 2. iTRVZ works as the signaling platform for various signaling pathways.

(**A**) Colocalization indices of various Halo7-tagged FA proteins with talin clusters. In the box plots throughout this report, bars, boxes, and whiskers indicate mean values, interquartile range (25–75%), and 10–90% range, respectively (n_{cells} = 20).

(**B**) Colocalization indices of the Halo7-tagged signaling molecules downstream of PDGFR with iTRVZ (n_{cells} = 20).

(**C**) Colocalization indices of PLCγ1-Halo7 and PLCβ1-Halo7 with iTRVZ after various stimulations, and the effects of FAK and SFK inhibitors (n_{cells} = 20).

(**D**) Dwell time of PLCγ1-Halo7 on iTRVZ; prolonged after stimulations (for τ_2, see the caption to **Figure 1**, n_{cells} = 20, n_{events} = 1,568, 3,894, and 5,232 for no stimulation, +CD59 clustering, and +PDGF, respectively).

(**E**) PDGF-induced increases of the PLCγ1-Halo7 number density (after/before PDGF) outside (bulk) and inside iTRVZ (dots for individual cells and mean ± SEM, n_{cells} = 10).

(**F**) Schematic drawing summarizing the characteristic properties of iTRVZ.

NS, not significant, *, P < 0.05, **, P < 0.01, using two-tailed Welch's t-test for (A and B), Games-Howell's test for (C), and Steel's test for (D).

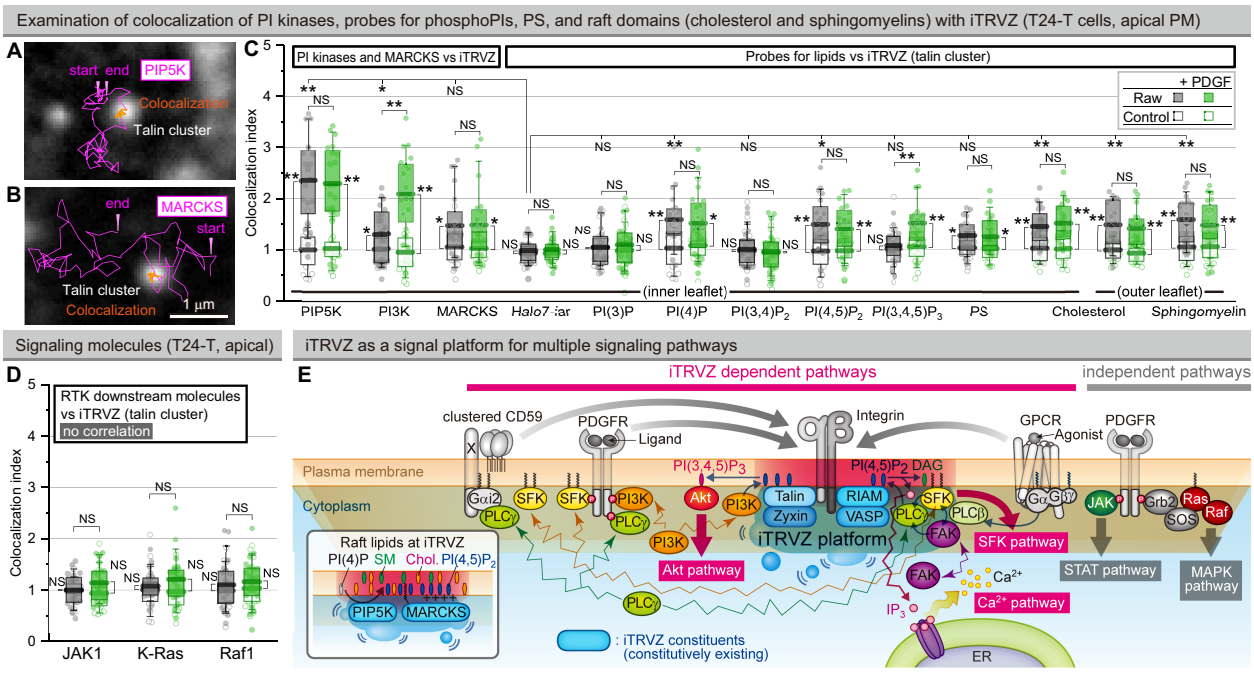

Fig. 3. PI kinases, some phosphoinositides, PS, and raft domains are colocalized with iTRVZ.

(**A** and **B**) PIP5K-Halo7 (A) and MARCKS-Halo7 (B) (trajectories) became transiently colocalized with talin clusters (white spots) (**movie S6**).

(**C**) Colocalization indices of Halo7-tagged PI kinases and lipid-binding probes with iTRVZ (data for PI3K are the same as those in **Figure 2B**, $n_{cells} = 20$).

(**D**) Colocalization indices of Halo7-tagged JAK1, K-Ras, and Raf1 with iTRVZ (no correlation, $n_{cells} = 20$).

(**E**) Schematic diagram summarizing various signaling processes occurring at iTRVZ.

NS, not significant, *, $P < 0.05$, **, $P < 0.01$, using two-tailed Welch's t-test for (C and D) and Games-Howell's test for (C).

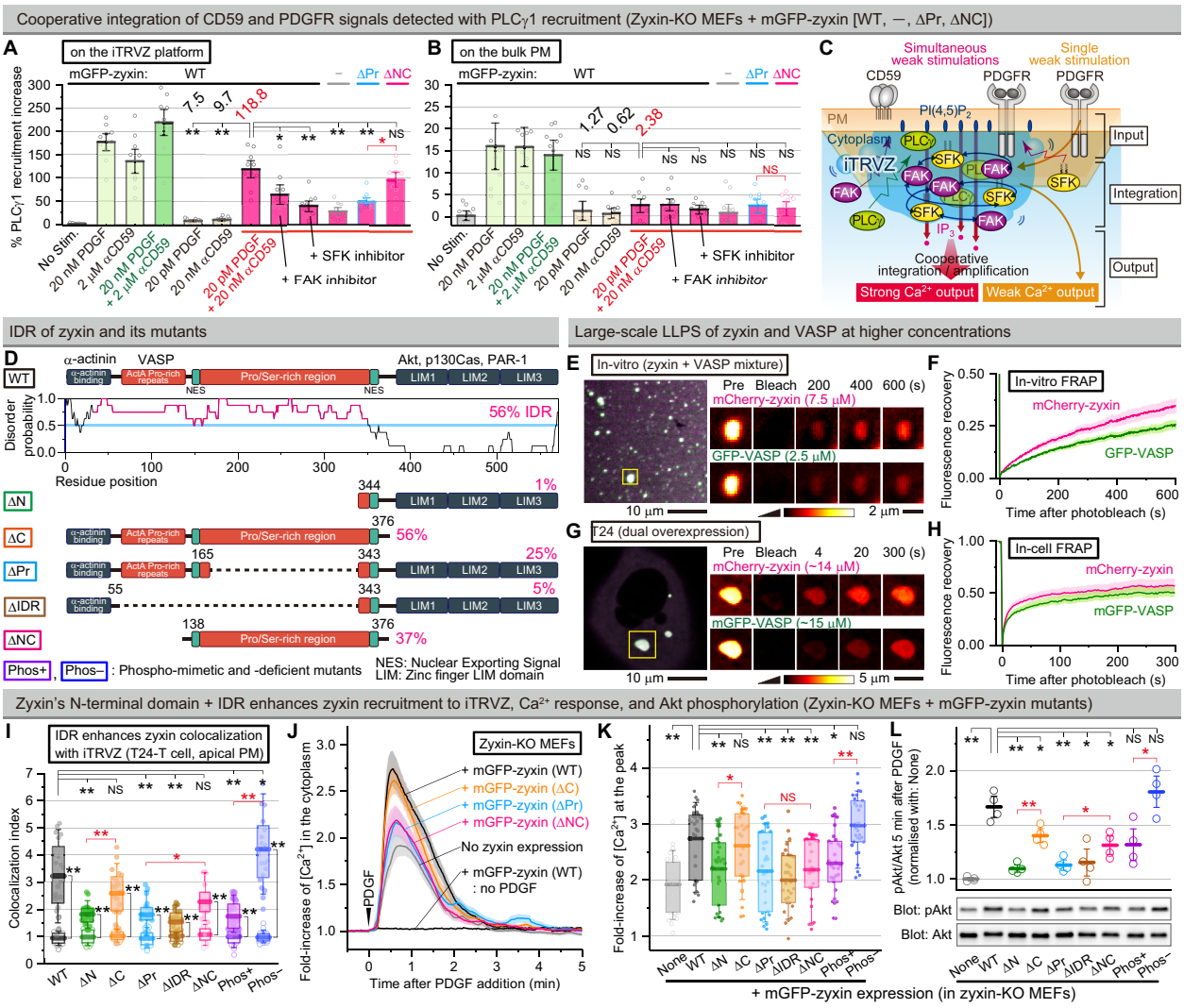

Fig. 4. iTRVZ works as a cooperative signal integrator and forms with the aid of LLPS by IDR interactions.

(**A** and **B**) % Increases of the total number of recruited PLCγ1-Halo7 on iTRVZ (A) and the bulk PM (B) after separate and simultaneous CD59 and PDGFR stimulations (n_{cells} = 10).

(**C**) Schematic figure showing that iTRVZ non-linearly integrates the CD59 and PDGFR signals by inducing cooperative interactions of FAK and SFK (**fig. S5E**).

(**D**) Domain structures of zyxin and its mutants used (predicted IDR in magenta).

(**E** to **H**) *In-vitro* ((E and F); 10 min after 1% PEG8K addition) and in-cell (G and H) FRAP of zyxin and VASP co-clusters (**movie S7**, $n_{droplets}$ = 15).

(**I**) Colocalization indices of Halo7-tagged zyxin mutants with iTRVZ (n_{cells} = 20).

(**J** and **K**) Ca^{2+} mobilization after PDGF stimulation. Typical time courses (J) and Fold increase at the peak (K) (n_{cells} = 30).

(**L**) Western blot analysis of PDGF-induced Akt phosphorylation ($n_{replicates}$ = 4).

NS, not significant, *, P < 0.05, **, P < 0.01, using Games-Howell's test for (A, B, I, K, and L) and two-tailed Welch's t-test for (I).